Experiments on Supersonic Fluid-Structure Interaction for an Incident Shock Configuration in the Wind Tunnel TMK

Dennis Daub
Sebastian Willems
Patrick Gruhn
Ali Gülhan
Deutsches Zentrum für Luft- und Raumfahrt e.V. (DLR), Institute of Aerodynamics and Flow Technology, Supersonic and Hypersonic Technologies Department, Linder Höhe, 51147 Köln, GERMANY

S. Michael Spottswood
Timothy Beberniss
Zachary Riley
Kirk Brouwer
Air Force Research Laboratory (AFRL), Structural Sciences Center (SSC), Wright-Patterson AFB, Ohio, USA

Dennis.Daub@dlr.de

ABSTRACT

Fluid-structure interaction (FSI) is a crucial problem in the design of supersonic and hypersonic vehicles but poses a substantial challenge for the modelling capabilities currently available. Cases that include shock-wave/boundary-layer interaction (SWBLI) are particularly challenging as the dynamics of such a flow field are not fully understood for cases with a rigid wall but typically include substantial low-frequency pressure fluctuations in the order of 1 kHz which is similar to the range of typical eigenfrequencies of vehicle surface structures. To improve understanding of such problems, we conducted experiments on supersonic FSI in combination with SWBLI in the wind tunnel TMK at DLR, Cologne. The experiments were conducted within project HYRECA in collaboration with the Air Force Research Laboratory (AFRL) Structural Sciences Center (SSC). We obtained large-amplitude self-excited oscillations of an elastic panel. Furthermore, the possibility of modifying the dynamic behavior of the structure by changing the Mach number during the wind tunnel run was explored. For the first time in the literature, the transient flow conditions were observed to induce drastic changes in the panel dynamics. Measurements of the structural dynamics were conducted both by using capacitive distance sensors inside the wind tunnel model and a Digital image correlation (DIC) system. The latter recorded full-field time-resolved surface deformation data. The results obtained in the present experiments are relevant and applicable both to supersonic and hypersonic configurations.

1.0 INTRODUCTION

Structural load conditions on the surface of super- and hypersonic vehicles can depend on the coupled behavior of the structure and the surrounding flow field. This can drastically increase both thermal and mechanical loads [1] [2] [3] [4]. The resulting behavior is often path-dependent and non-linear (e.g. [5] [6]). The X-15 supersonic research aircraft is an instructive example. It's surface structures experienced thermal buckling, melting due to incident shock heating, and flutter dynamics [7] [8] [9]. The latter led to cracks in surface panels on the vehicle. The reliable prediction of such loads requires consideration of the coupled behavior of flow field and vehicle structure and still poses a substantial challenge for numerical modelling.

The focus of this study is on the mechanical loads for a panel structure that may be driven by flutter, by intrinsic dynamics of a flow field with shock-wave/boundary-layer interaction (SWBLI), or by prescribed movements of an incident shock. In addition to this, the effect of transients of the flow conditions is explored by changing the Mach number during the wind tunnel runs. These phenomena are studied in a collaborative effort using wind tunnel experiments and complementary numerical modelling. This will enable the detailed study of the behavior of such a coupled configuration and validation of the numerical models by comparison to experimental data in a range of conditions where the coupled dynamic behavior is still not fully understood and that remains challenging for numerical modelling. This paper describes the experimental part of the ongoing work.

1.1 Shock-Wave/Boundary-Layer interaction (SWBLI)

In cases where an incident shock impinges on a boundary layer, the pressure rise across the shock may cause the boundary layer to separate (e.g. [10]). This is referred to as SWBLI. In such a flow field, a shock forms upstream of the separated area which is also upstream of the inviscid impingement location of the incident shock. This leads to a mean pressure rise upstream of the incident shock. Additionally, the resulting system shows a broad range of localized dynamics. Most notably, substantial dynamics can occur at frequencies well below 1000 Hz which is typically in a similar range as the natural frequencies of panel structures of flight vehicles. Importantly, such dynamics can currently only reliably be modelled using high-fidelity models such as Large eddy simulations (LES) (e.g. [11]). See [3] [12] for a discussion of SWBLI on a rigid wall for the present configuration.

1.2 Fluid-Structure Interaction (FSI)

Generally, the behavior of a structure depends on its mass, stiffness, and damping, which has to be considered together with the mounting and support structure. Stiffness and damping along with structural deformations can depend on the thermal state of the structure and also on mechanical load conditions. This means they can be influenced by heating from the flow field as well as by pressure loads. Vice versa, the flow field may be influenced by the thermal state of the structure, mean deformation, and structural dynamics [1] [3].

Certain combinations of dynamic pressure and panel properties (i.e. mass and stiffness) lead to self-excited oscillations of surface panels [13]. This can occur in cases with and without SWBLI. It has been shown numerically and also experimentally that the presence of an incident shock can in some cases drastically lower the level of dynamic pressure required to obtain flutter [1] [4] [6].

In addition to this, structural dynamics may also be induced by the intrinsic low-frequencies dynamics of SWBLI in cases where flutter does not occur. This has been observed both for incident shock and ramp configurations [1] [14] [15]. Also, the properties of the SWBLI were observed to have an influence of flutter dynamics [3] [16] [17].

2.0 EXPERIMENTAL SETUP

This section provides an overview of the wind tunnel, the experimental setup, and instrumentation.

2.1 Wind Tunnel TMK

To obtain supersonic flow conditions at high Reynolds numbers, the experiments were conducted in the Trisonic Wind Tunnel TMK of the Supersonic and Hypersonic Technologies Department at DLR, Cologne (Figure 1, Figure 2). TMK is a blow-down facility with a Mach number range of 0.5 to 5.7. The Reynolds number can be varied by using a heater or adjusting total pressure. The pressure range can be extended by using an ejector system. The heater is also required to prevent condensation at high Mach numbers. The test section has a rectangular cross section of 0.6 m × 0.6 m. The nozzle contour is variable and can be altered during the wind tunnel run. For transonic flow, a special test section with perforated walls has to be used.

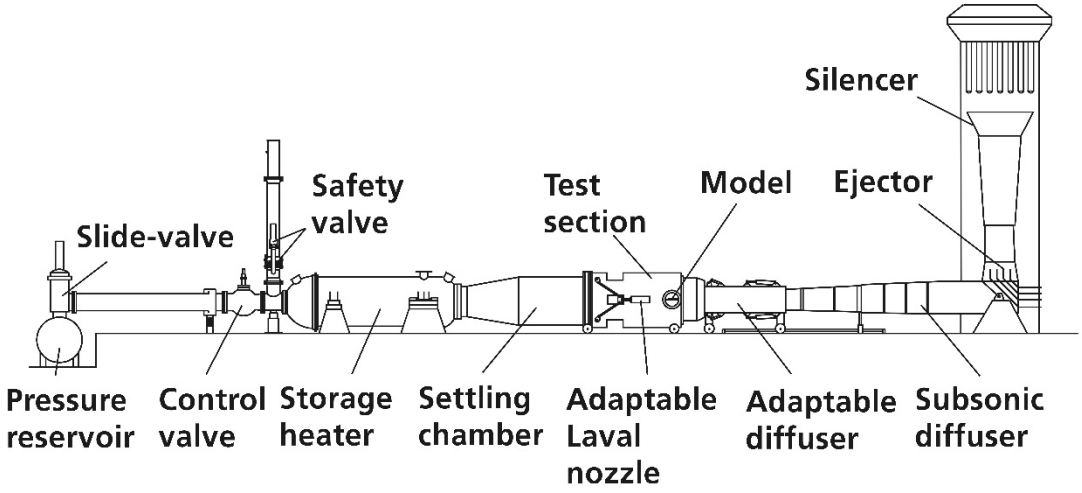

Figure 1: Schematic of the wind tunnel TMK at DLR, Cologne

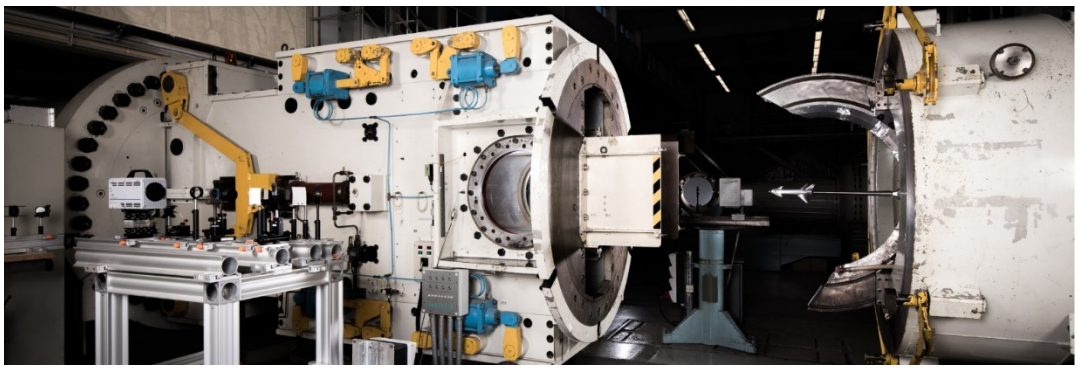

Figure 2: Nozzle and test section of the wind tunnel TMK at DLR, Cologne

2.2 Flow Conditions

The flow conditions for this study were chosen to investigate the effects of flutter and SWBLI dynamics on a thin panel. Conditions were selected for which no significant aerothermal heating of the panel is expected. Cases with combinations of flutter, SWBLI, and thermal buckling of thin elastic panels at a Mach number 5.3 conducted in the wind tunnel H2K at DLR, Cologne showed complicated interdependencies of these mechanisms including a drastic effect of very small temperature changes on structural dynamics [2] [3]. For such combined cases, it is difficult to identify the individual contributions of these mechanisms on the

resulting behavior, especially considering that not even the SWBLI-intrinsic dynamics on a rigid surface are fully understood. Table 1 shows typical TMK flow conditions. This study considered conditions at Mach 3 and 4 as well as variable Mach number entries (between Mach 3 and 4) to obtain a "trajectory-like" change in flow conditions. The latter can be obtained by adjusting the nozzle contour during a wind tunnel run.

Table 1: Typical Flow Conditions in TMK

Ma	p_0	T_0	p_{inf}	T_{inf}	u_{inf}	Re_{inf}
3.0	582 kPa	293 K	15.5 kPa	104 K	616 m/s	$44 \cdot 10^6$ /m
4.0	1374 kPa	293 K	8.7 kPa	69 K	671 m/s	$61 \cdot 10^6$ /m
5.0	2050 kPa	370 K	3.9 kPa	62 K	787 m/s	$40 \cdot 10^6$ /m

2.3 Wind Tunnel Model

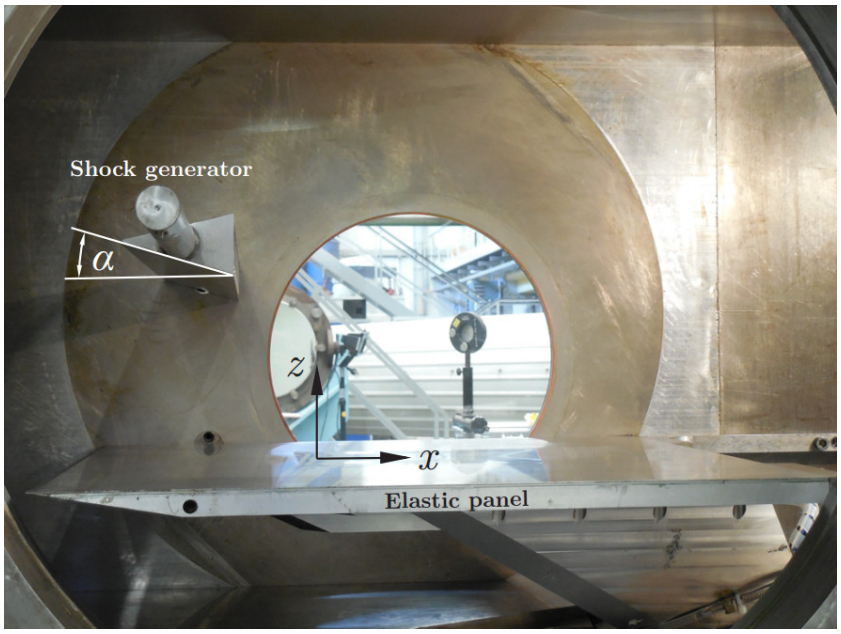

Figure 3: Sideview of wind tunnel model [3]

The wind tunnel model consists of a flat plate with a sharp leading edge that holds the elastic and rigid reference panels and a rotatable shock generator (see Figure 3). While the shock generator position is fixed, the impingement location of the generated shock can be varied by rotating the shock generator or adjusting the Mach number. The rotatable shock generator is outfitted with a servo drive that can rotate the shock generator within the limits of drive torque and inertia of the system (Figure 4). Furthermore, it can hold position at any desired angle. Thus, the shock generator can be used to excite panel dynamics by its own movement (see [14]), but can also be used at a steady angle to observe flutter effects or effects of the intrinsic SWBLI dynamics.

The wind tunnel model was designed such that a free/unsupported area of the panel of 300 mm x 200 mm can be used for FSI studies. The elastic panel used for the present experiments was machined from a solid piece by AFRL. A panel thickness of 0.61 mm was achieved. The panel surface is slightly wavy from the manufacturing process and was measured by AFRL.

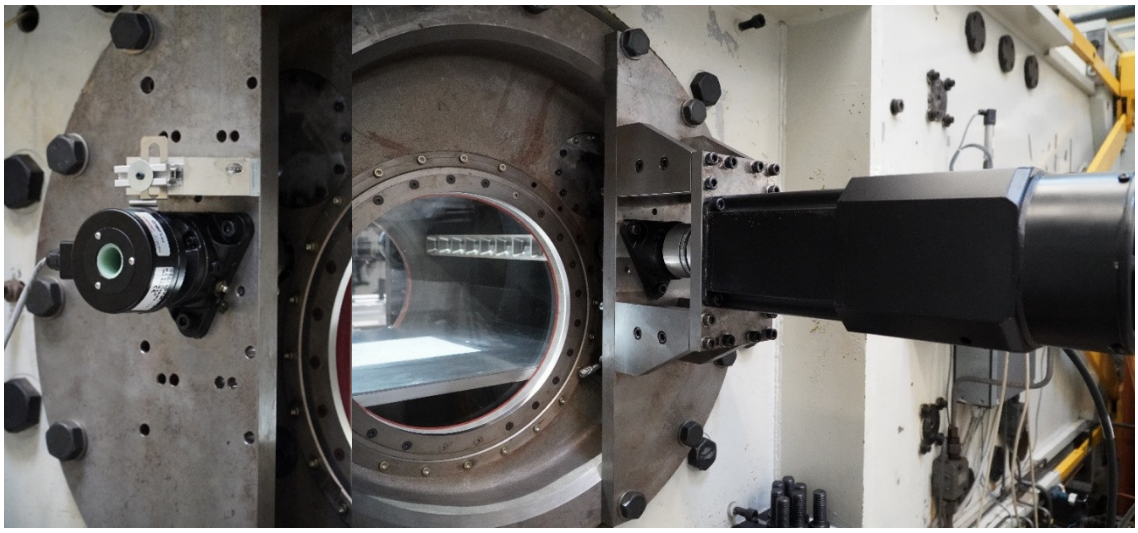

Figure 4: Incremental encoder and drive assembly

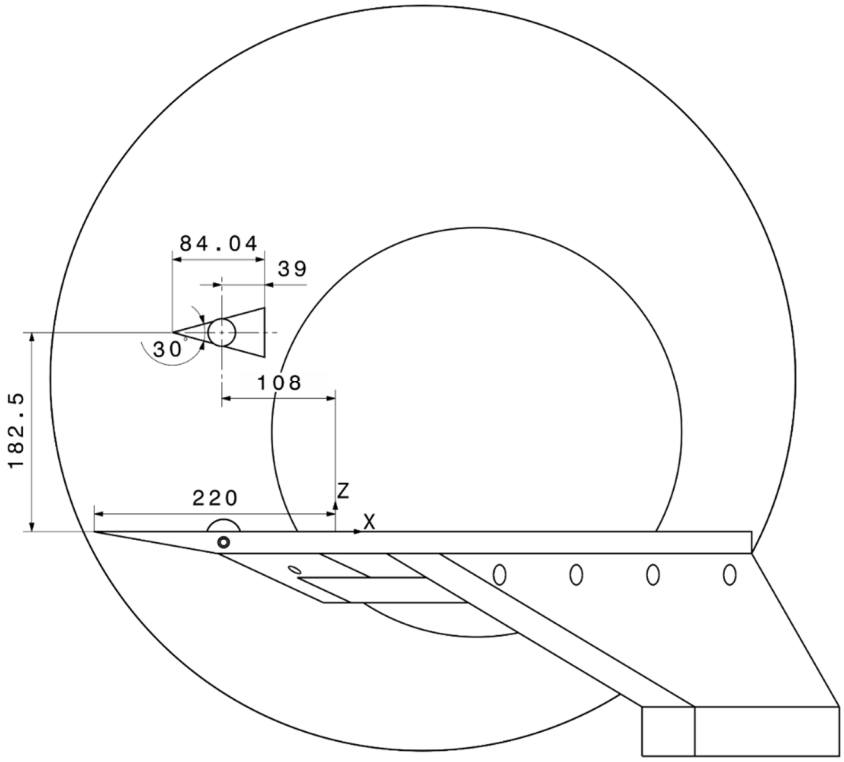

Figure 5: Shock generator and wind tunnel model geometry [3]

Figure 5 shows the geometry of the rotatable shock generator that is positioned at x = -108 mm and z = 182.5 mm (center of the shaft). The coordinate system used throughout this study is located at the upstream end of the free panel area.

The pressure underneath the panel, or cavity pressure, is an important boundary condition. In a previous study in TMK, the cavity underneath the panel was connected to a static pressure port upstream of the test section. The pressure rise across the SWBLI caused a large mean deformation and thus drastically increased the stiffness of the structure which strongly reduced panel dynamics [4]. For the present experiments, the cavity was connected to a vacuum system outside TMK that enabled setting the cavity pressure to the desired level before the wind tunnel run. Such a system had proven to work well in the wind tunnel H2K [4] and was successfully adapted to the TMK facility.

2.4 Instrumentation

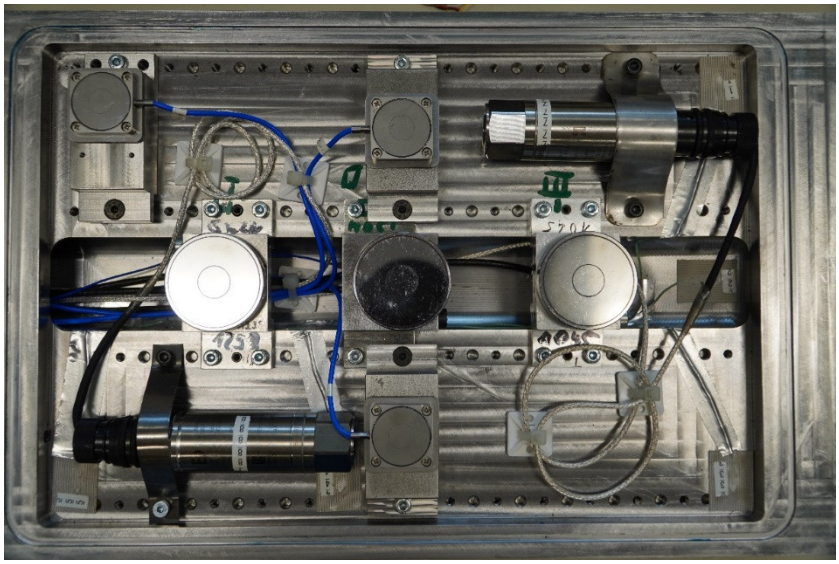

Figure 6: Capacitive distance sensors underneath the elastic panel

Table 2: Micro-Epsilon capacitive distance sensors

Sensor Type	Position	x /mm	y /mm
CS5	front	75	0
CS5	center	150	0
CS5	rear	225	0
CSH3FL	left	150	62
CSH3FL	right	150	-62
CSH3FL	corner	270	-72

Figure 7: DIC system box and cameras (flow from right)

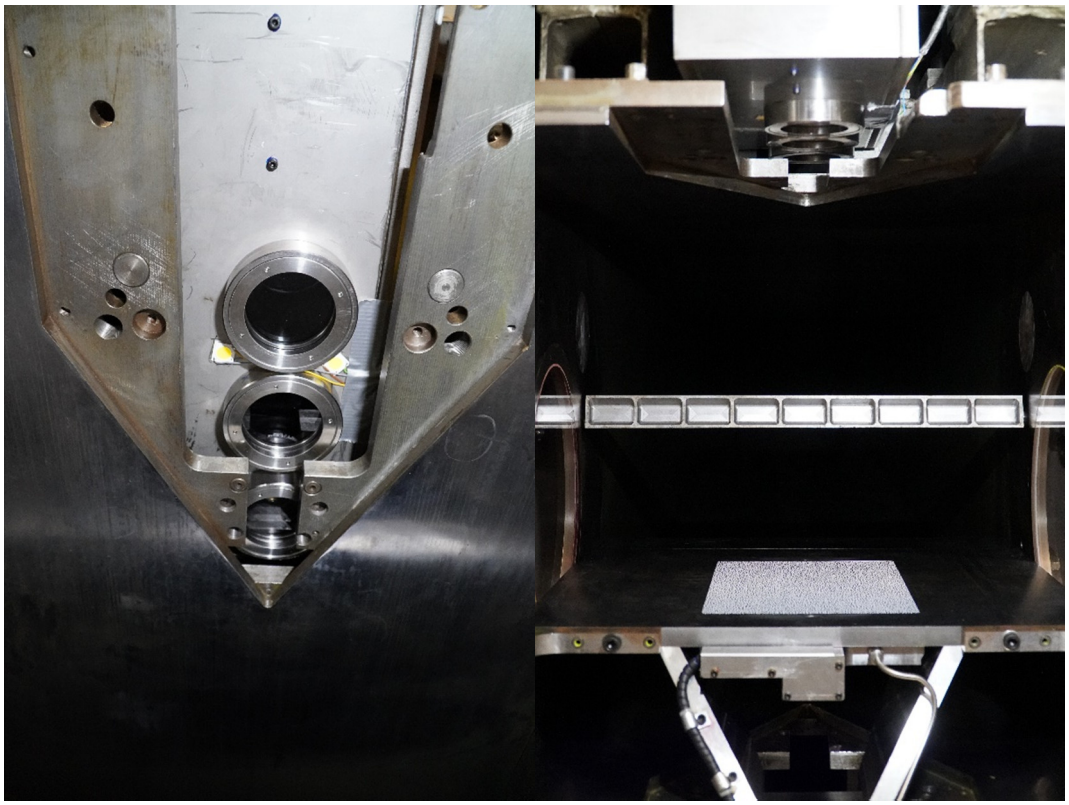

Figure 8: Position of the DIC box in the wind tunnel TMK

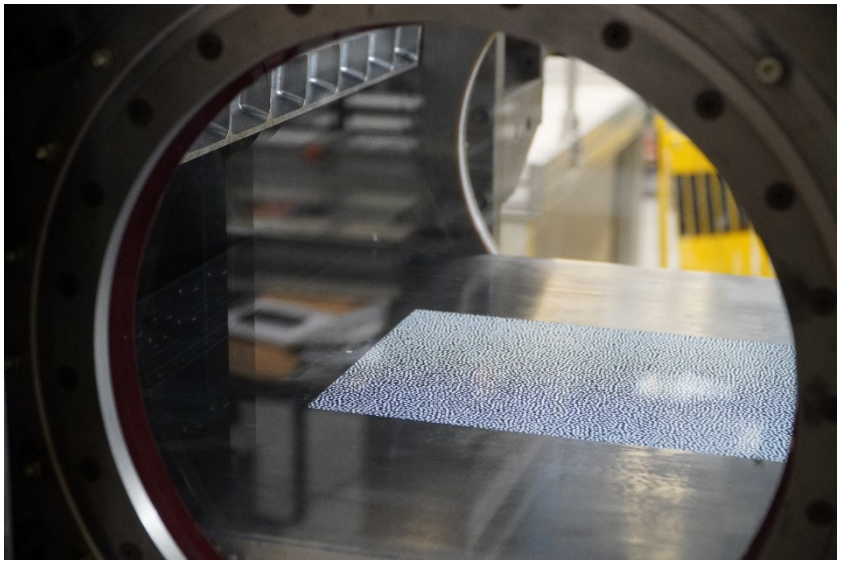

Figure 9: Elastic panel with DIC pattern mounted in the TMK test section

The deformation of the elastic panels was measured by capacitive distance sensors and a Digital image correlation (DIC) system. The capacitive distances sensors (Figure 6) are an upgraded version of the system used in a previous study [5]. Uncertainty could be reduced relative to the previous setup by an improved calibration. The measurement ranges and number of channels were adjusted to acquire more data on panel positions off the center line. The sensor positions are given in Table 2. This system is ideally suited for validation of the DIC system that has not previously been used at TMK. The capacitive distance sensors were placed underneath the elastic panel inside the wind tunnel model while the DIC system measures on the flow-exposed wall of the elastic structure. The options for suitable optical access are quite limited at TMK, but a solution was found to position the DIC system overhead the test section of the wind tunnel. Figure 7 and Figure 8 show the DIC box and its location overhead the test section. Since DIC can be sensitive to density gradients in the flow field the comparison to the capacitive measurement system in these challenging conditions will be particularly valuable. The high-speed, stereo DIC setup consisted of two Photron AX-200 cameras with 32 GB of RAM (Figure 7). Mounted to the Photrons were two Nikon 20 mm lens with aperture of f/4.0. The image sample rate was 2500 fps with a shutter speed to match causing the shutter to be open during the entire frame. The shutter speed was kept as close to the frame rate as possible to minimize the likelihood of temporal aliasing. The aperture was kept as open as possible to minimize the depth of focus as a means to avoid optical distortions resulting from density gradients [18]. Typically, the camera angle is evenly divided between the two cameras, however, due to limited optical access the upstream camera was placed directly over and perpendicular to the panel specimen and the downstream camera was rotated the entire nominal 25° camera angle. Due to the large angle of the downstream camera the largest lens aperture of 2.8/f was not possible to keep the entire panel length in focus therefore f/4.0 was a compromise. Correlated Solutions Vic3D was used for calibration and correlation of the high-speed images. A 25mm Correlated Solutions combined DIC panel was used to calibrate the system. Calibration results were a pixel deviation of 0.037 and a calculated camera angle of 22 degrees. The DIC speckle pattern was created with white and black, flat finish, high-heat spray paint. The dots were produced using an adhesively back vinyl stencil. The stencil pattern is created with a Matlab script that optimizes the pattern for the particular application. With the combination of the optical settings and the stencil, the dots were on average 4 pixels in diameter. The DIC cameras were viewing the panel through a rectangular cutout in the

test section top wall (Figure 8). The cutout terminates with a triangular shape that created a partially obstructed view for the upstream camera. The top wall of the test section moves up and down when the free stream Mach number is changed and therefore the obstructed view increased and decreased with a change in Mach number. The correlation used subsets 31 pixels in size with an overlap of 7 pixels. There was approximately 1.9 pixels per millimeter. Spectral proper orthogonal decomposition (SPOD) results for various runs at select frequencies are included in the following results. The out-of-plane displacement (z) magnitude is arbitrary [19]. Time intervals of a duration of one second were used for the computation.

The flow field was recorded using a Z-type Schlieren setup. For the present configuration, this has the drawback that the view of the flow field in the center of the test section can be obstructed by the flow structure near the side walls. For future campaigns, a self-aligned focusing Schlieren system will be set up to solve this problem [20]. Nevertheless, the present setup provides valuable qualitative information on the state of the flow field.

3.0 EXPERIMENTAL RESULTS

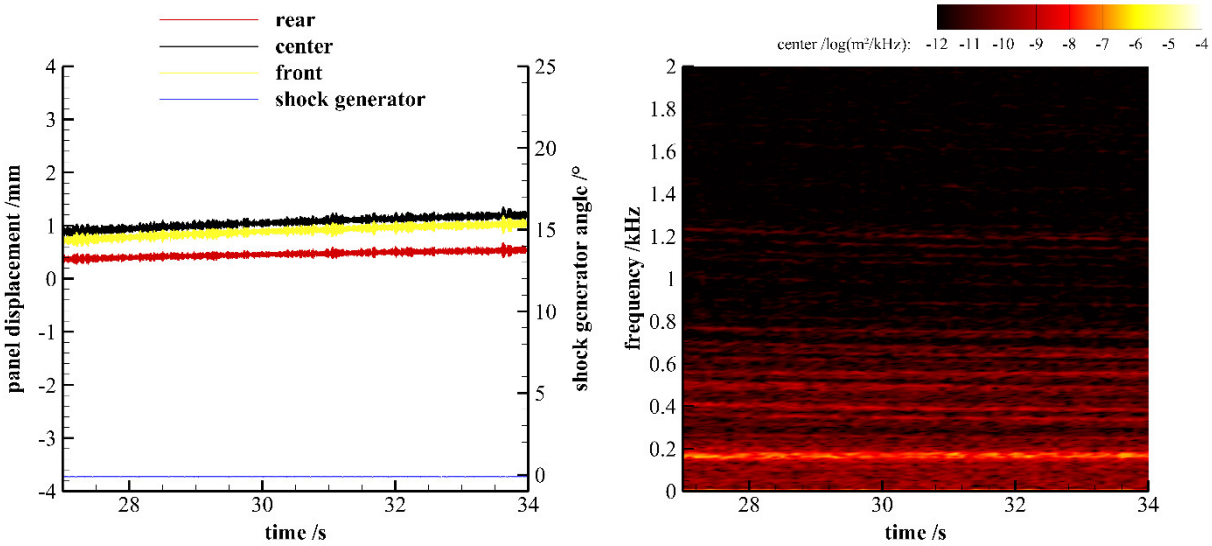

Figure 10: Displacement of the elastic panel (left) and PSD of center displacement (right) at M=3 without incident shock (run 11)

Figure 10 shows the measured panel displacement at several locations under the panel and the Power spectral density (PSD) of the displacement at the panel center for a wind tunnel run at M=3 without incident shock. The PSD shows the power distribution over a frequency range, e.g. enables visualizing at which frequencies relevant oscillations occur. For the M=3 flow condition, panel dynamics only take place at very low amplitudes. The cavity pressure is set such that no large mean deformation takes place. Small variations of the cavity pressure were also investigated in additional runs, but no case with larger amplitude dynamics could be obtained at this flow condition without incident shock.

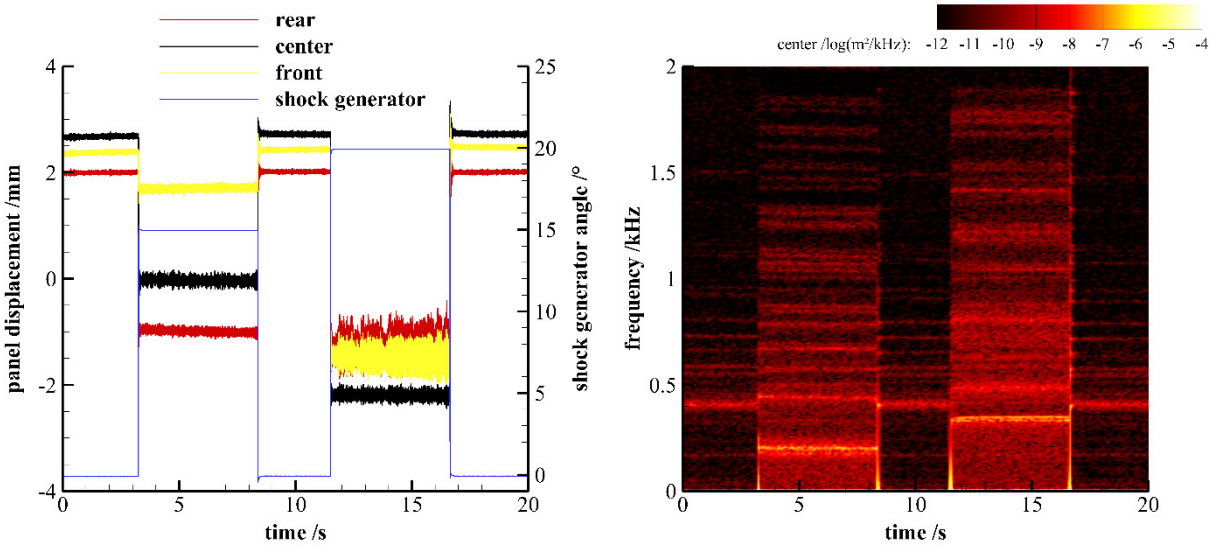

Figure 11: Displacement of the elastic panel (left) and PSD of center displacement (right) at M=3, cavity pressure≈17.4 kPa, with shock generator at 15° and 20° (run 18)

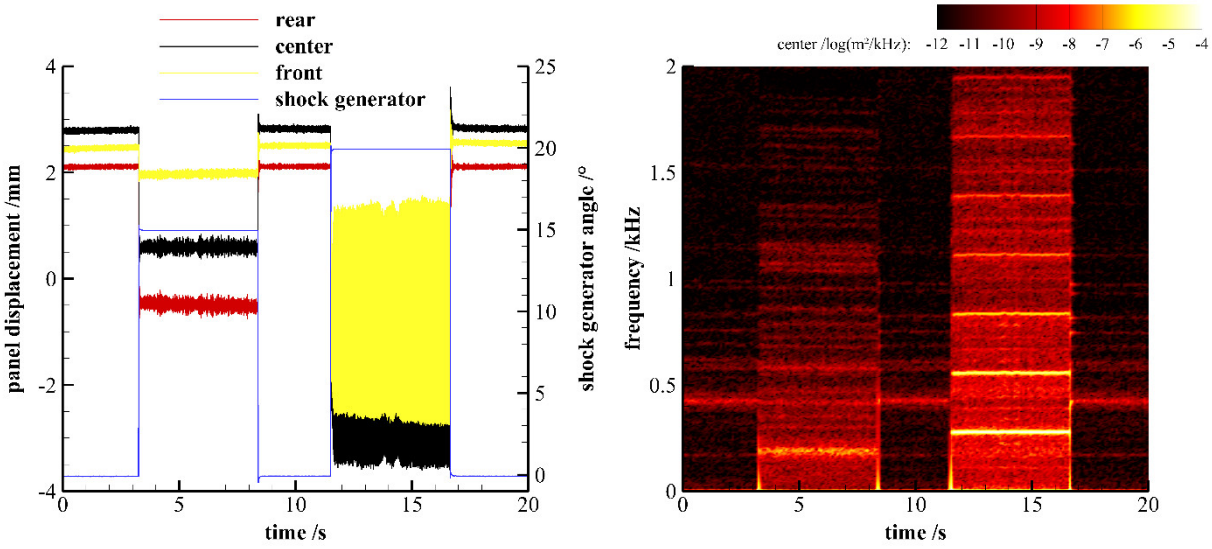

Figure 12: Displacement of the elastic panel (left) and PSD of center displacement (right) at M=3, cavity pressure≈36.4 kPa, with shock generator at 15° and 20° (run 17)

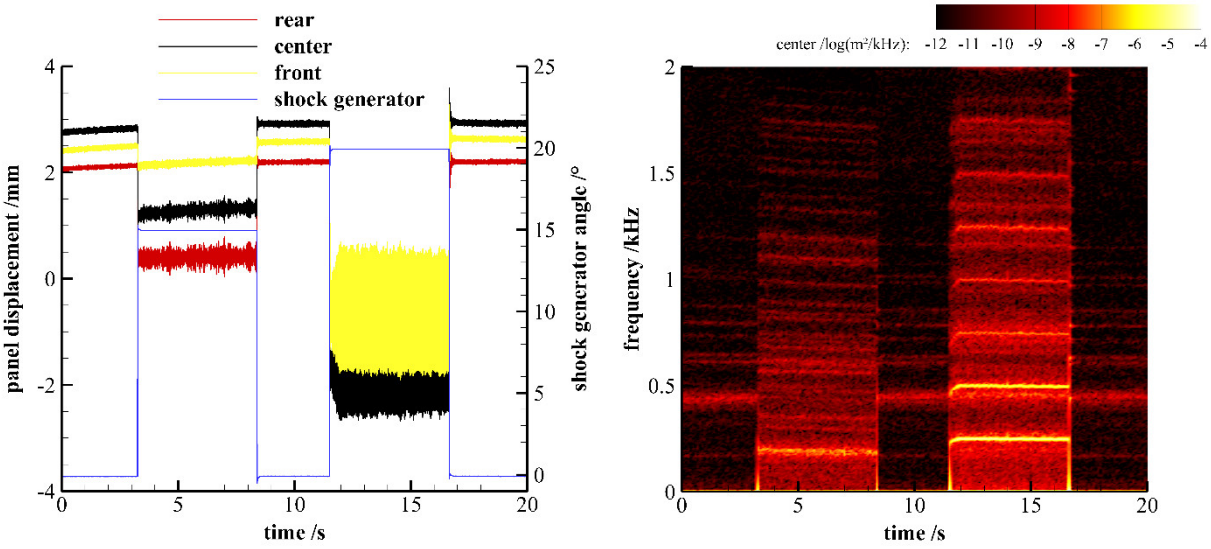

Figure 13: Displacement of the elastic panel (left) and PSD of center displacement (right) at M=3, cavity pressure≈39.5 kPa, with shock generator at 15° and 20° (run 20)

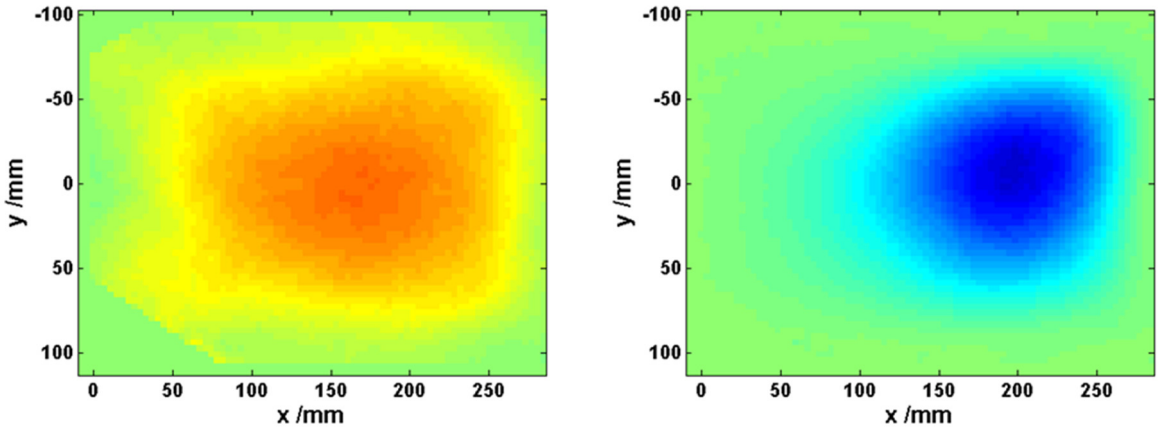

Figure 14: Run 20 SPOD 1 sec, no shock, 430 Hz (left); 5 sec, 15° shock, 195 Hz (right)

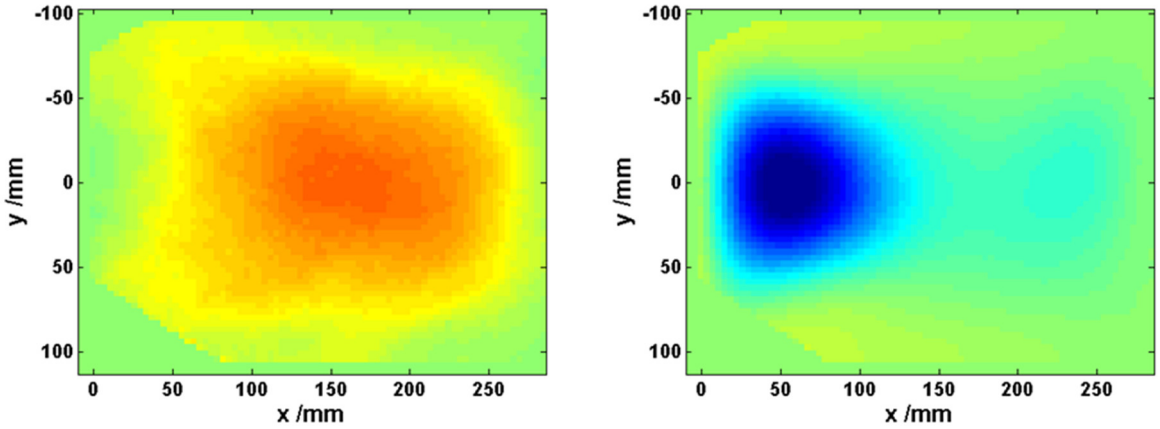

Figure 15: Run 20 SPOD 10 sec, no shock, 430 Hz (left); 15 sec, 20° shock, 250 Hz (right)

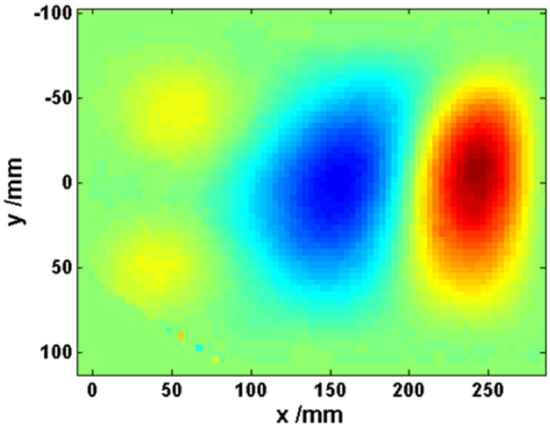

Figure 16: Run 20 SPOD 15 sec, 20° shock, 499 Hz

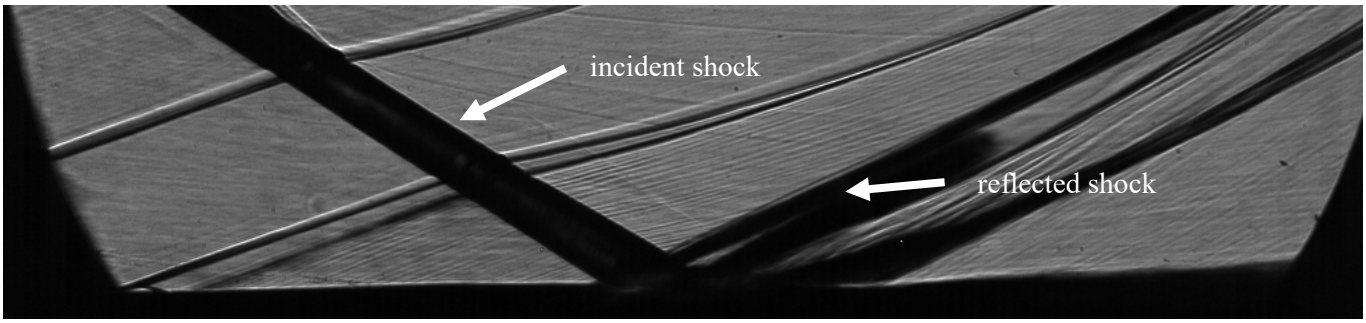

Figure 17: Flow field at M=3 with 15° shock generator angle

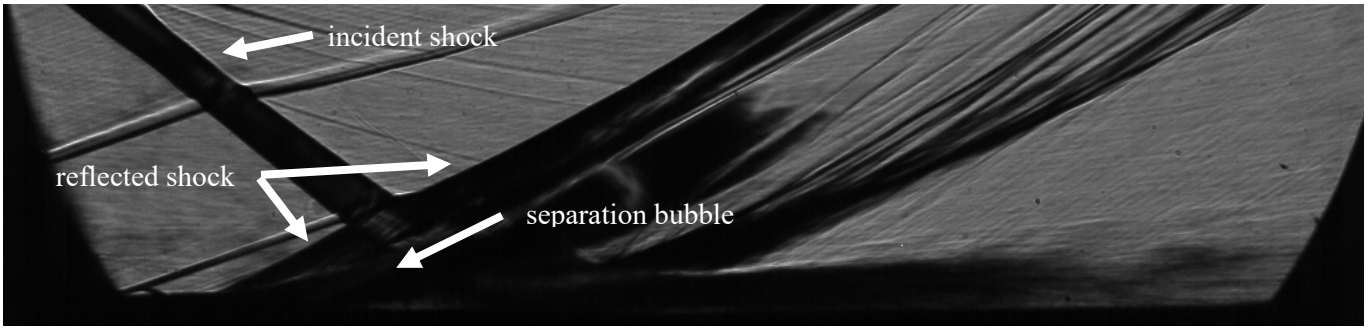

Figure 18: Flow field at M=4 with 20° shock generator angle

The following figures (Figure 11 to Figure 21) show the measured panel displacement at several locations under the panel, the PSD of the displacement at the panel center, and SPOD modes for cases where the shock generator was used to create an incident shock. The wind tunnel was running at the M=3 condition and initially there was no incident shock on the panel. In each of these runs, the shock generator was then quickly rotated to a ramp angle of 15°, left at this position for several seconds, and then returned to 0° (no shock on the panel). Next, the shock generator was rotated to a ramp angle of 20°, again left in this position for several seconds, then rotated back to 0° for shutdown of the flow. The cavity pressure is given for the state before the incident shock moves onto the panel. Figure 17 and Figure 18 show examples of Schlieren images of the respective flow fields. It can be seen that the occurring flow separation is much larger and the impingement locations is further upstream for the case with 20° shock generator angle. The flow conditions are the same for all the runs shown. The only variation is in the cavity pressure underneath the panel. It can be seen that for the lowest cavity pressure (Figure 11) some dynamics occur for a 20° shock generator angle. With the next step in cavity pressure (Figure 12), the amplitude of the dynamics observed for 20° shock generator angle drastically increases. Interestingly, for a further increase in cavity pressure (Figure 13), substantial dynamics are still taking place, however, at a somewhat lower amplitude compared to the previous case. This shows how sensitive the coupled configuration is to the boundary condition set by the cavity pressure, and also that there is a certain combination of cavity pressure and flow properties for which maximum dynamics occur. Both if the cavity pressure is higher or lower than that dynamics are reduced. Generally, the dynamics observed in the time series plots are also reflected in the PSD plots of the center displacement sensor. It is particularly notable, that during large amplitude dynamics at 20° shock generator angle peaks in amplitude at multiple discreet frequencies can be observed which are probably harmonics of the lowest detected frequency (e.g. Figure 12). To further investigate the occurring dynamics, SPOD modes at selected frequency peaks were computed (Figure 14 – Figure 16) for run 20 (Figure 13). In Figure 14 and Figure 15, the left images show the SPOD mode without incident shock loading whereas the right plots show the first SPOD mode with the incident shock on the panel. Interestingly, the mode shape changes differently depending on the incident shock loading with the incident shock location for 15° shock generator angle being downstream of the shock impingement location for the 20° case. In both cases, the modes with incident shock loading occur at a much lower frequency than in the state without incident shock loading. For the 20° case, Figure 16 shows the SPOD mode occurring at twice the frequency of the lowest frequency peak, presumably a harmonic.

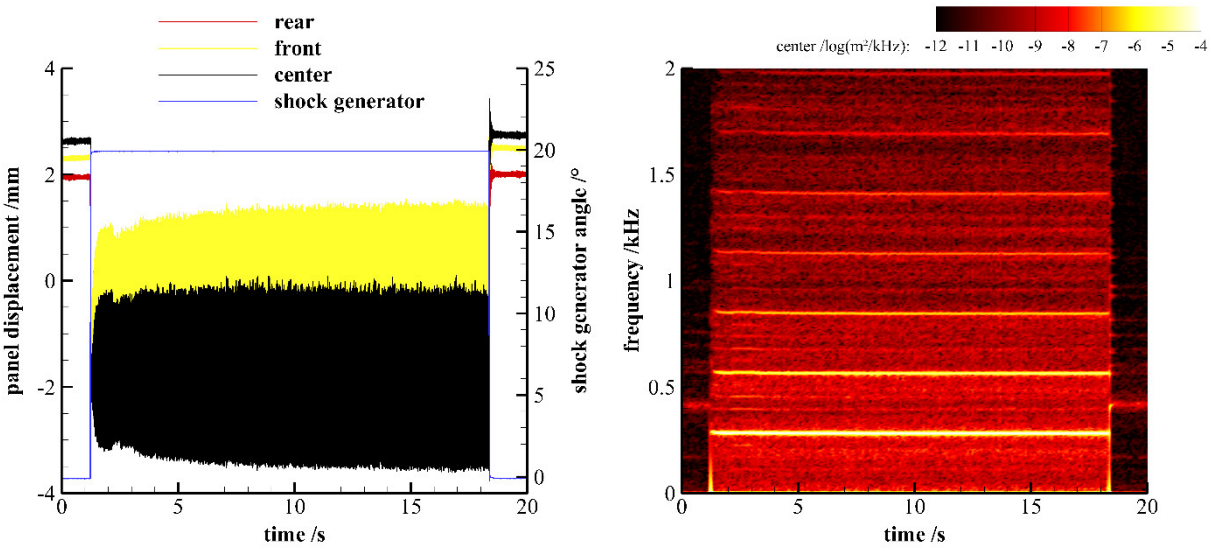

Figure 19: Displacement of the elastic panel (left) and PSD of center displacement (right) at M=3, cavity pressure≈35.5 kPa, with shock generator at 20° (run 24)

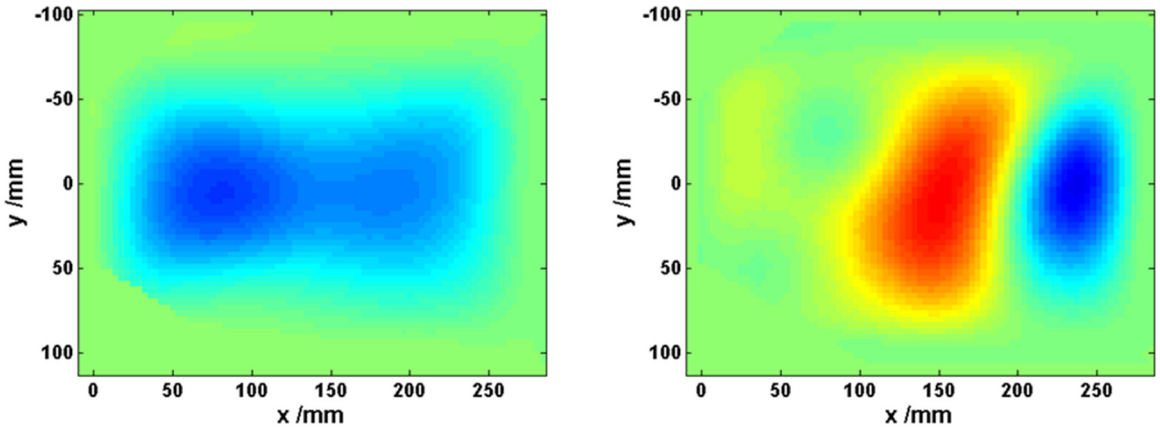

Figure 20: Run 24 SPOD 5 sec, 282 Hz (left); 5 sec, 564 Hz (right)

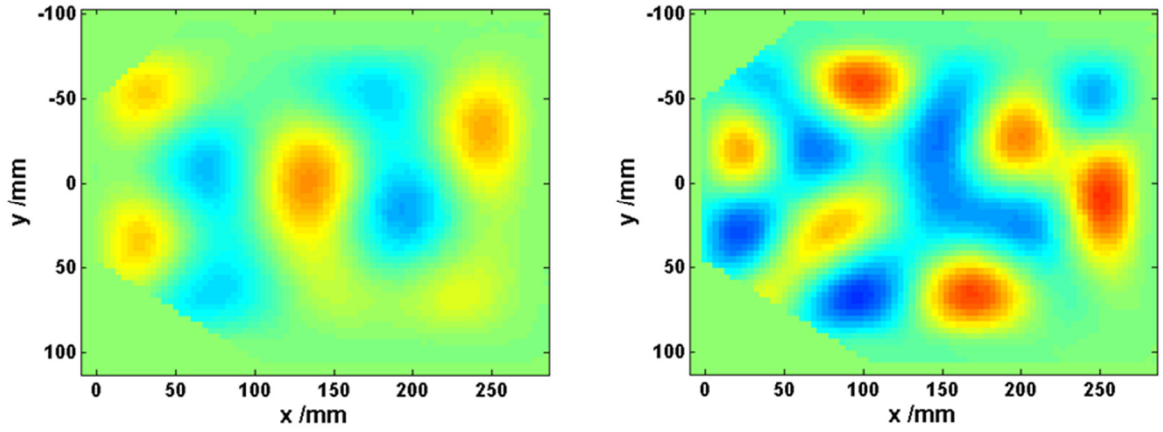

Figure 21: Run 24 SPOD 5 sec, 846 Hz (left); 5 sec, 1128 Hz (right)

Figure 19 shows a long-duration run at the M=3 flow condition and 20° shock generator angle maintaining large-amplitude dynamics of the panel for more than 15 seconds. This did not lead to any obvious damage of the panel structure but would be expected to eventually lead to structural failure if continued. The SPOD modes for the lower frequencies shown in Figure 20 match the observation previously made for a similar configuration (see Figure 14 and Figure 15). Figure 21 shows the more complicated pattern emerging at higher frequencies.

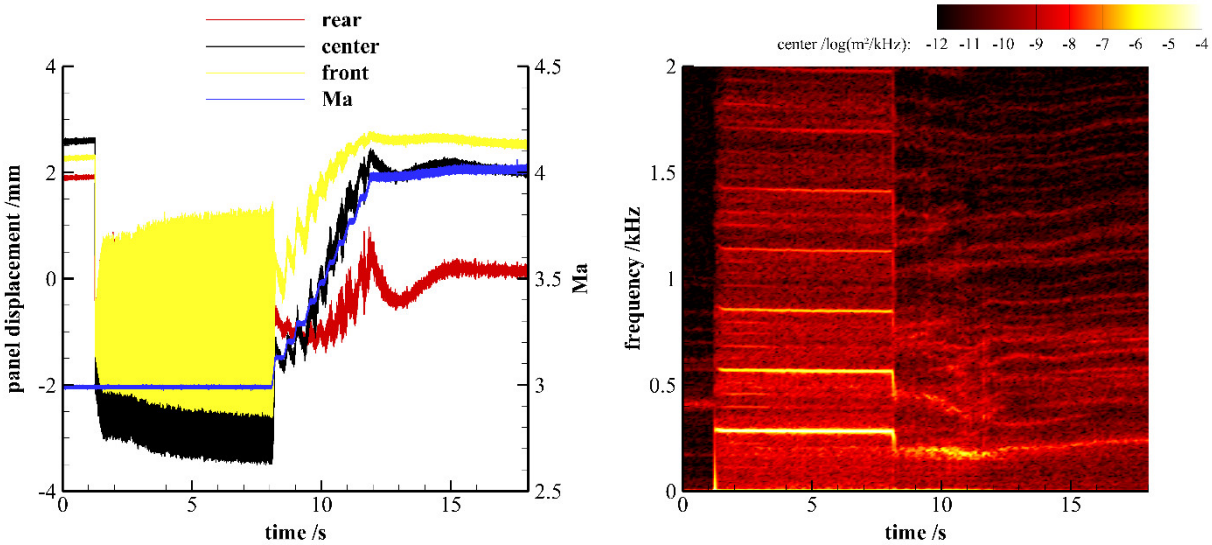

Figure 22: Displacement of the elastic panel (left) and PSD of center displacement (right) at M=3 to M=4, cavity pressure≈35.4 kPa, with shock generator at 20° (run 23)

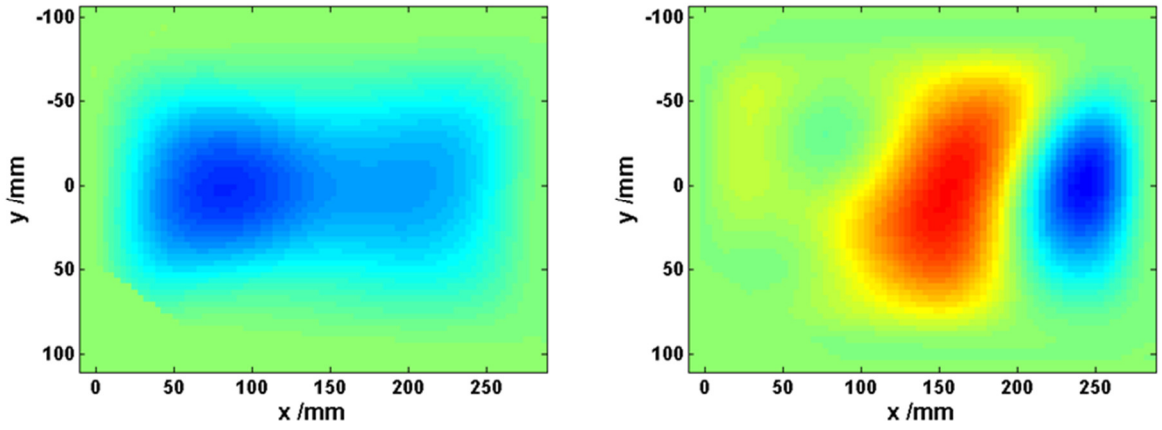

Figure 23: Run 23 SPOD 5 sec, Mach 3, 283 Hz (left); 5 sec, Mach 3, 566 Hz (right)

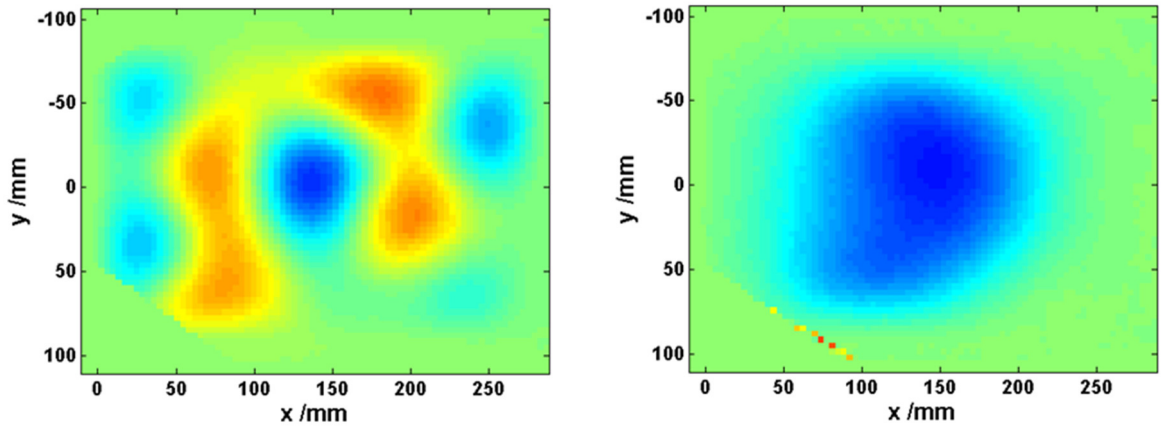

Figure 24: Run 23 SPOD 5 sec, Mach 3, 849 Hz (left); 10 sec, Mach 3 to 4, 0 Hz (right)

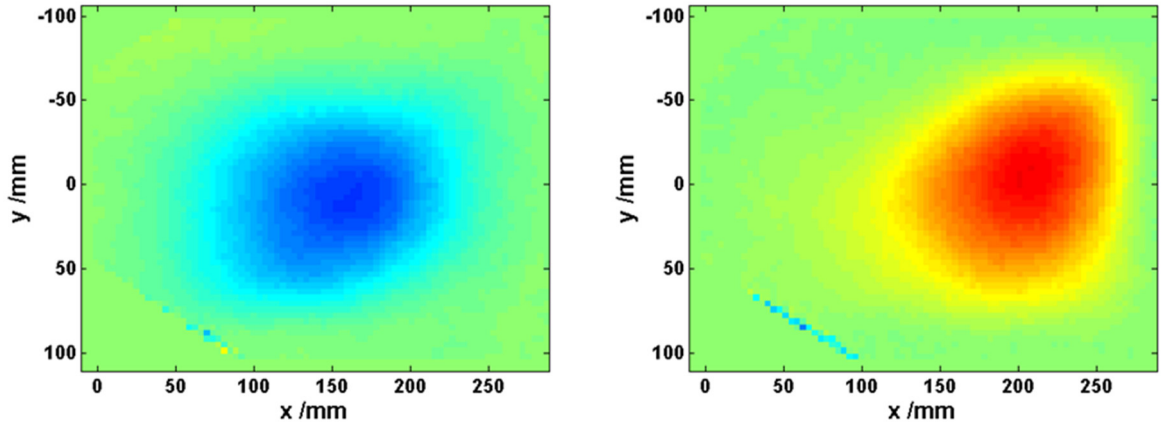

Figure 25: Run 23 SPOD 10 sec, Mach 3 to 4, 195 Hz (left); 16 sec, Mach 4, 231 Hz (right)

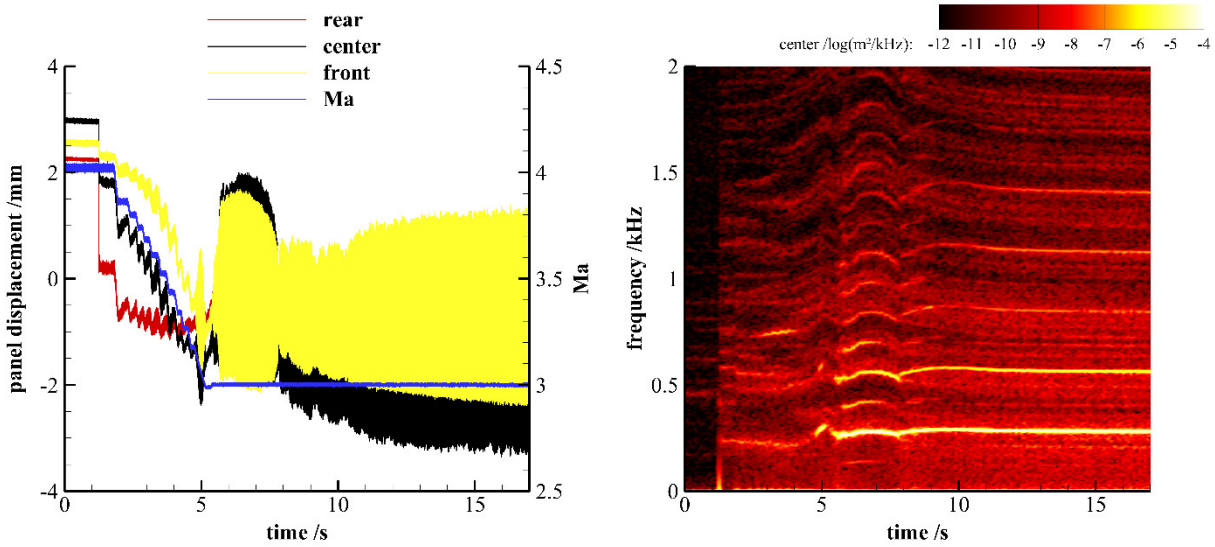

Figure 26: Displacement of the elastic panel (left) and PSD of center displacement (right) at M=4 to M=3, cavity pressure≈36.3 kPa, with shock generator at 20° (run 22)

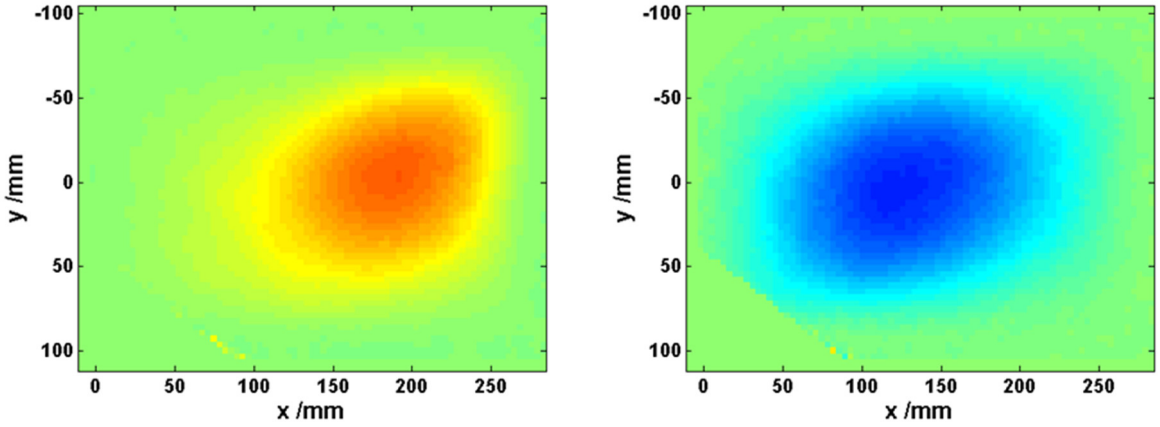

Figure 27: Run 22 SPOD 1.5 sec, Mach 4, 236 Hz (left); 3 sec, Mach 4 to 3, 220 Hz (right)

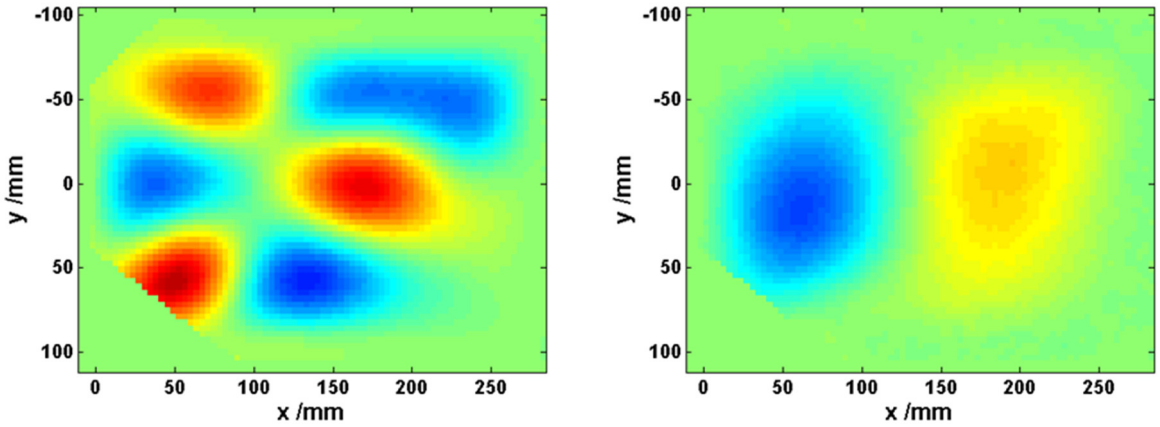

Figure 28: Run 22 SPOD 3 sec, Mach 4 to 3, 744 Hz (left); 6 sec, Mach 3, 140 Hz (right)

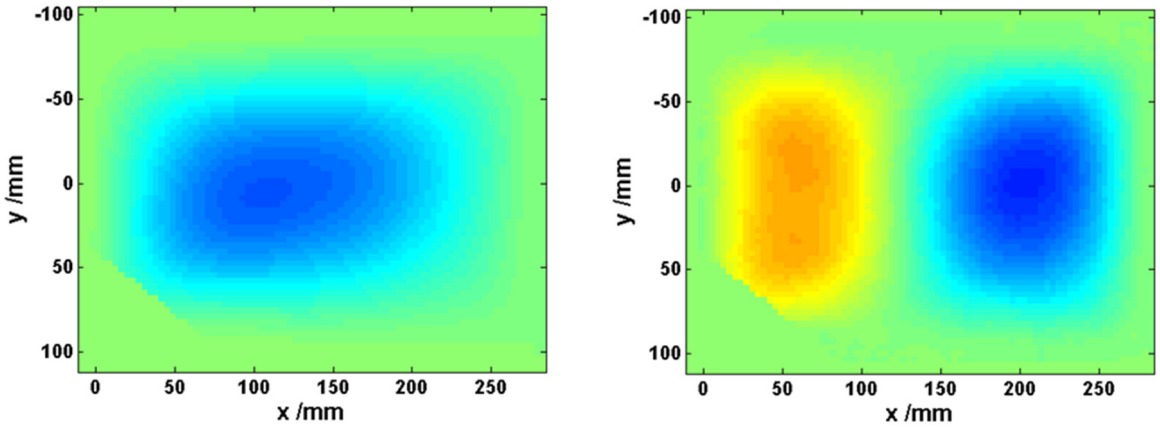

Figure 29: Run 22 SPOD 6 sec, Mach 3, 280 Hz (left); 6 sec, Mach 3, 420 Hz (right)

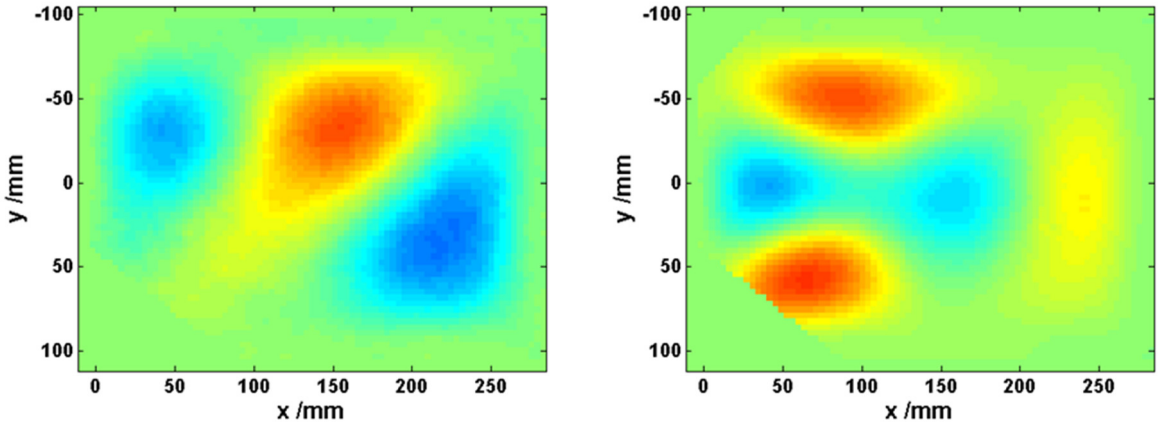

Figure 30: Run 22 SPOD 6 sec, Mach 3, 560 Hz (left); 6 sec, Mach 3, 700 Hz (right)

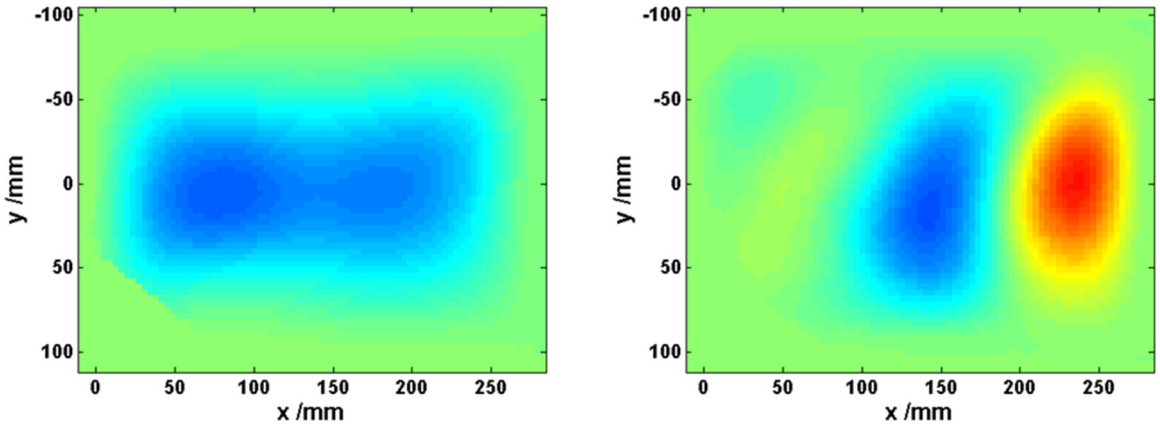

Figure 31: Run 22 SPOD 15 sec, Mach 3, 280 Hz (left); 15 sec, Mach 3, 560 Hz (right)

Figure 22 and Figure 26 show results from wind tunnel runs where the Mach number was adjusted during the run. For Figure 22, the Mach number was initially 3 and then was changed to 4. For Figure 26, the Mach number was initially 4 and was changed to 3. For both cases, the shock generator is used at 20°. Very interestingly, panel dynamics react immediately to the change in Mach number. Figure 23 – Figure 25 and Figure 27 – Figure 31 show the respective SPOD modes at various points in time during these transient cases. For the conditions at the beginning of run 23 (Figure 23) and at the end of run 22 (Figure 31) at Mach 3 with 20° shock generator angle, the SPOD modes are similar to the steady cases (e.g. run 24, Figure 20). At the end of run 23 (Figure 25) and the beginning of run 22 (
Figure 27) at Mach 4 and 20° shock generator angle the observed SPOD modes are also very similar between both transient runs. However, the transient behaviour in between shows differences depending on the direction of the transient (Figure 24, Figure 29, Figure 30). It should be noted that the transient in Mach number is accompanied by a change in total pressure. This also changes the free stream pressure. Consequently, this and the change in shock strength and impingement location change the pressure distribution of the SWBLI flow field on the panel. The cavity pressure was not adjusted during the Mach number change. Because of this and the changes in the flow field the pressure difference across the panel changes. This complex combination of transient changes influencing the FSI configuration will be analysed further during the remainder of the project. To the authors' collective knowledge, no similar results have been reported in the literature.

3.0 CONCLUSION

During this experimental campaign conducted in the wind tunnel TMK at DLR, Cologne, large amplitude oscillations of a panel subjected to an SWBLI flow field were obtained. In addition to conventional instrumentation, DIC was successfully used for the first time in this facility to obtain full field time-resolved records of the panel deformation by measuring through the flow field. The reaction of the coupled configuration to changes in the incident shock angle and the cavity pressure were explored extending the very limited data base of results on such coupled configurations. In addition to observations under steady conditions, the reaction of the coupled configuration to transient changes in flow conditions was explored using the capability of the wind tunnel TMK to quickly change the Mach number during a wind tunnel run.

A drastic reaction of the panel dynamics to changes in the inflow Mach number during the wind tunnel run could be demonstrated. This is a completely novel addition to the literature and is highly relevant to the behavior of real structures under flight loads that are inherently transient.

ACKNOWLEDGEMENTS

The authors gratefully acknowledge the help and advice of the technical staff of the Supersonic and Hypersonic Technologies Department. This research was conducted in project HYRECA funded by BAAINBw.

BIBLIOGRAPHY

[1] S. M. Spottswood, T. J. Beberniss, T. G. Eason, R. A. Perez, J. M. Donbar, D. A. Ehrhardt und Z. B. Riley, „Exploring the response of a thin, flexible panel to shock-turbulent boundary-layer interactions," *Journal of Sound and Vibration,* Bd. 443, p. 74–89, March 2019.

[2] D. Daub, B. Esser und A. Gülhan, „Experiments on High-Temperature Hypersonic Fluid-Structure Interaction with Plastic Deformation," *AIAA Journal,* Bd. 58, p. 1423–1431, April 2020.

[3] D. Daub, „DLR-FB 2023-09: Experimental Investigation of Supersonic Fluid-Structure Interaction for Future Space Transportation Systems," DLR, Köln, 2023.

[4] D. Daub, S. Willems und A. Gülhan, „Experiments on aerothermoelastic fluid-structure interaction in hypersonic flow," *Journal of Sound and Vibration,* 2022.

[5] M. Freydin, E. H. Dowell, S. M. Spottswood und R. A. Perez, „Nonlinear dynamics and flutter of plate and cavity in response to supersonic wind tunnel start," *Nonlinear Dynamics,* July 2020.

[6] M. R. Visbal, „On the interaction of an oblique shock with a flexible panel," *Journal of Fluids and Structures,* Bd. 30, p. 219–225, April 2012.

[7] W. H. Stillwell, „X-15 Research Results - With a Selected Bibliography," Washington, D.C., 1965.

[8] G. H. Jordan, N. J. McLeod und L. D. Guy, „Structural Dynamic Experiences of the X-15 Airplane," Flight Research Center, Edwards, Ca., 1962.

[9] J. D. Watts, „Flight Experience with Shock Impingement and Interference Heating on the X-15-2 Research Airplane," Flight Research Center, Edwards, Ca., 1968.

[10] D. S. Dolling, „Fifty Years of Shock-Wave/Boundary-Layer Interaction Research: What Next?," *AIAA Journal,* Bd. 39, p. 1517–1531, August 2001.

[11] V. Pasquariello, S. Hickel und N. A. Adams, „Unsteady effects of strong shock-wave/boundary-layer interaction at high Reynolds number," *Journal of Fluid Mechanics,* Bd. 823, pp. 617-657, 2017.

[12] D. Daub, S. Willems und A. Gülhan, „Experimental results on unsteady shock-wave\boundary-layer interaction induced by an impinging shock," *CEAS Space Journal,* 2016.

[13] E. H. Dowell, Aeroelasticity of Plates and Shells, L. Meirovitch, Hrsg., Leyden, Netherlands: Noordhoff International Publishing, 1975.

[14] D. Daub, S. Willems und A. Gülhan, „Experiments on the Interaction of a Fast-Moving Shock with an Elastic Panel," *AIAA Journal,* Bd. 54, p. 670–678, February 2016.

[15] T. J. Whalen, A. G. Schöneich, S. J. Laurence, B. T. Sullivan, D. J. Bodony, M. Freydin, E. H. Dowell und G. M. Buck, „Hypersonic Fluid–Structure Interactions in Compression Corner Shock-Wave/Boundary-Layer Interaction," *AIAA Journal,* Bd. 58, p. 4090–4105, September 2020.

[16] N. R. Boyer, J. J. McNamara, D. V. Gaitonde, C. J. Barnes und M. R. Visbal, „Features of panel flutter response to shock boundary layer interactions," *Journal of Fluids and Structures,* Bd. 101, p. 103207, February 2021.

[17] K. Brouwer, R. Perez, T. Beberniss und S. M. Spottswood, „Aeroelastic response of a thin panel excited by a separated shock–boundary layer interaction," *Physics of Fluids,* 2023.

[18] T. Beberniss und D. Ehrhardt, „Visible Light Refraction Effects on High-Speed Stereo Digital Image Correlation Measurement of a Thin Panel in Mach 2 Flow," *Experimental Techniques,* 2020.

[19] A. Towne, O. Schmidt und T. Colonius, „Spectral proper orthogonal decomposition and its relationship to dynamic mode decomposition and resolvent analysis," *Journal of Fluid Mechanics,* 2018.

[20] J. Weisberger und B. Bathel, „Single source/cutoff grid, self-aligned focusing schlieren system," *Experiments in Fluids,* 2022.